Improvement on Doppler Reconstruction in Multiprobe OTA Setups for Directional-Antenna Devices

Lijian Xin, *Member, IEEE*, Yong Li, *Member, IEEE*, Cheng-Xiang Wang, *Fellow, IEEE*, Jie Huang, *Member, IEEE*, and Ronghui Zhang, *Member, IEEE*

***Abstract*—This article proposes an improved channel reconstruction method to increase the accuracy of Doppler emulations when measuring directional multi-antenna devices in over-the-air (OTA) testing at millimeter wave (mmWave) bands. In real radio channels, the Doppler spectrum depends on incoming ray angles. In OTA testing, the target Doppler spectrum is accurately created when assessing omni-directional antenna terminals using the conventional prefaded signal synthesis (PFS) method. However, the devices under test (DUTs) may consist of directional antennas that produce different gains in impinging angles. Since the PFS method ignores the dependence of the Doppler spectrum on the DUT antenna element pattern, it will lead to inaccurate channel emulation, thus affecting the link performance of the DUT. Therefore, an improved PFS method is proposed by considering the impact of the DUT antenna element pattern. Specifically, the rays within a cluster mapped to active probes are divided into multiple subsets, each of which is weighted to synthesize the cluster. The objective function with constraints between the target temporal covariance and emulated one is established to obtain all subset weights. Simulation results verify that the proposed channel emulation method is superior to the existing PFS technique for Doppler emulation while not degrading the emulated spatial characteristics using the proposed optimization strategy.**

***Index Terms*—Channel emulation, Doppler spectrum, optimization, spatial covariance, temporal covariance.**

Manuscript received 31 October 2022; revised 22 February 2023 and 30 May 2023; accepted 8 July 2023. Date of publication 1 August 2023; date of current version 19 December 2023. This work was supported in part by the National Natural Science Foundation of China under Grants 61971067, 61960206006, and 61901109, in part by the Key Technologies R&D Program of Jiangsu (Prospective and Key Technologies for Industry) under Grants BE2022067 and BE2022067-4, in part by the EU H2020 RISE TESTBED2 project under Grant 872172, in part by the High Level Innovation and Entrepreneurial Doctor Introduction Program in Jiangsu under Grant JSSCBS20210082, in part by the Start-up Research Fund of Southeast University under Grant RF1028623029, in part by the Fundamental Research Funds for the Central Universities under Grant 2242023K5003, and in part by the China Postdoctoral Science Foundation under Grant 2023M730341. The review of this article was coordinated by Prof. Vittorio Degli-Esposti. *(Corresponding author: Yong Li.)*

Lijian Xin is with the Pervasive Communication Research Center, Purple Mountain Laboratories, Nanjing 211111, China (e-mail: xinlijian@pmlabs.com.cn).

Yong Li is with the Key Laboratory of Universal Wireless Communications (Ministry of Education), Beijing University of Posts and Telecommunications, Beijing 100876, China (e-mail: liyong@bupt.edu.cn).

Cheng-Xiang Wang and Jie Huang are with the National Mobile Communications Research Laboratory, School of Information Science and Engineering, Southeast University, Nanjing 210096, China, and also with the Pervasive Communication Research Center, Purple Mountain Laboratories, Nanjing 211111, China (e-mail: chxwang@seu.edu.cn; j_huang@seu.edu.cn).

Ronghui Zhang is with the State Key Laboratory of Networking and Switching Technology, Beijing University of Posts and Telecommunications, Beijing 100876, China (e-mail: ronghzhang@bupt.edu.cn).

Digital Object Identifier 10.1109/TVT.2023.3299257

I. Introduction

Over-the-air (OTA) testing provides a viable way to measure the performance of multi-antenna terminals in a controlled laboratory environment. This method is more feasible and repeatable than field testing under realistic propagation environments. Compared with conducted testing for mobile devices, OTA testing has the advantages of no need to break the devices under test (DUTs) and including the impact of the antenna on the radiated performance of DUTs. Moreover, conducted testing will no longer be applicable for measuring massive multiple-input multiple-output (MIMO) devices owing to demanding the same number of cable connections to its antenna ports. For millimeter-wave (mmWave) antenna systems that are highly integrated without accessible antenna ports, conducted testing also fails to work. Therefore, the OTA testing method, such as the multiprobe anechoic chamber (MPAC) setup, has been extensively researched and developed to measure the performance of the MIMO terminals [1].

The cluster-based channel modeling has been used to model wireless multipath channels [2], [3]. Each cluster has a specific angular power spectral density (PSD) and delay. The MPAC method is capable of recreating the channel multipath characteristics in a controlled laboratory [4], [5], [6], [7], including the prefaded signal synthesis (PFS) technique and the plane wave synthesis (PWS) technique. The channel emulation models for these two methods were introduced to measure multi-antenna devices in [4]. The spatial-correlation function can describe the spatial properties of channels, which depends on the angular PSD and the antenna radiation pattern [8], [9]. Hence, the spatial characteristics of the emulated channel were evaluated by measuring the spatial-correlations among antennas in the test area [5], [6], [7]. In [10], the whole spatial covariance matrix was considered to emulate the power imbalance among the antennas-under-test rather than the spatial-correlation based metric. In [11] and [12], the impact of the DUT antenna pattern on the spatial-correlation for emulation was investigated. Furthermore, the massive MIMO has been widely employed as an enabling technology for the fifth generation (5 G) [13]. Compared with the MIMO OTA testing, the physical dimension of the MPAC setup and the system link budget need to be considered in massive MIMO OTA testing. The actual MPAC setups applied to assess massive MIMO devices were studied in [14], [15], [16], [17]. Moreover, an MPAC setup for evaluating mmWave devices was proposed and a power weighting method was further provided in [18]. In [19], a probe weighting strategy based on angular spectrum similarity was proposed, which can be used to evaluate the beamforming of massive MIMO base stations (BSs).

Since the non-linearity switches and power amplifiers, unstable phase caused by long-term phase drift, and ambient temperature changes have large impacts, it is difficult to guarantee the phase coherence of probes when measuring massive MIMO devices, especially at mmWave bands. Therefore, the PFS method is more promising than the PWS technique in massive MIMO OTA testing due to without calibrating probe phases [4]. In realistic radio channels, the terminal antenna elements with different directivity will result in different Doppler profiles due to their impacts. However, this cannot be accurately reproduced using the PFS method unless the DUT antenna element patterns are omni-directional in the MPAC setup. The reason is that the identically distributed fading sequences between probes are required to synthesize clusters, which neglects the dependence of the Doppler spectrum on antenna element patterns of the DUTs. In summary, the Doppler profile of the emulated channel under the conventional PFS method is inaccurate in MIMO OTA testing for directional-antenna terminals. Hence, the link performance of the DUT, such as system throughput, will be affected. However, the defect of the PFS method was neglected when evaluating multiple antenna devices in existing works [4], [5], [6], [7], [14], [15], [16], [17], [18], [19]. Unlike these works, this article proposes an improved channel emulation method and establishes an objective function. The threefold contributions of this article are as follows.

- The problem that the Doppler profile for channel emulation is inaccurate using the conventional PFS method is demonstrated and analyzed when measuring the DUT with directional antennas in massive MIMO OTA testing. Hence, an improved channel emulation method is proposed. Specifically, the rays within a cluster mapped to active probes are divided into multiple ray subsets, each of which is weighted to synthesize the overall cluster.
- The temporal covariance functions are derived for the target channel, the emulated channel using the conventional PFS method, and the improved channel emulation model. Then, the temporal covariance deviation function considering constraints is structured for determining the optimal weights of ray subsets. The Doppler profile for channel emulation is improved without compromising the emulated spatial properties.
- The temporal correlations of different channel emulation methods are compared under various simulation scenarios with an operating frequency of 28 GHz. Moreover, the impacts of the number of active probes and the number of rays on the Doppler emulation are also studied.

The rest of this article is organized as follows. A target channel model, an emulated channel model using the conventional PFS method, and an improved channel emulation model are introduced in Section II. Section III derives the spatial covariances and the temporal covariances of these three channel models. Furthermore, an optimization strategy is proposed to obtain the weights of probe antennas and ray subsets. Simulation validations are shown in Section IV. Finally, conclusions are drawn in Section V.

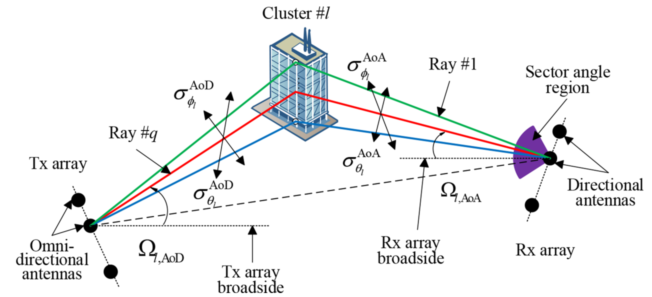

Fig. 1. Spatial structure of a GBSM.

Notations: The transpose, the conjugate, and the Hermitian operators are defined as $(\cdot)^{\mathrm{T}}$, $(\cdot)^*$, and $(\cdot)^{\mathrm{H}}$, respectively. $\|\cdot\|_1$ represents the ℓ_1-norm, and $\|\cdot\|_2$ denotes the ℓ_2-norm. The expectation operator is defined as $\mathbf{E}\{\cdot\}$, the symbol '$\cdot$' is the scalar product operation, and the symbol '$\iff$' denotes the sure equivalence.

II. Channel Models

A. Target Channel Model

Among various channel models, geometry-based stochastic models (GBSMs) are usually used to represent MIMO channels and separate the transmitter (Tx) and receiver (Rx) antenna patterns from the propagation parameters [2], [20]. A GBSM consists of several clusters, each of which has specific channel parameters, as shown in Fig. 1. The mean angle of departure (AoD) and angle of arrival (AoA) for the lth cluster are defined as $\Omega_{l,\text{AoD}}$ and $\Omega_{l,\text{AoA}}$, respectively. The azimuth angle spread of departure (ASD), elevation angle spread of departure (ESD), azimuth angle spread of arrival (ASA), and elevation angle spread of arrival (ESA) of the lth cluster are characterized by $\sigma^{\text{AoD}}_{\phi_l}$, $\sigma^{\text{AoD}}_{\theta_l}$, $\sigma^{\text{AoA}}_{\phi_l}$, and $\sigma^{\text{AoA}}_{\theta_l}$, respectively. In the uplink, the omni-directional antenna terminal is located on the Tx side. The directional multi-antenna device covering a sectorized spatial region is located on the Rx side.

Let's assume that the Rx antennas and Tx antennas are located in the far-field of electromagnetic radiation, and the numbers of the Rx antenna elements and Tx antenna elements are U and S, respectively. A MIMO channel can be written as the matrix $\mathbf{H}_{\text{tar}}(t,\tau) = \{h_{u,s}(t,\tau)\} \in \mathbb{C}^{U\times S}$, where $\mathbb{C}$ represents the complex number. The time-variant channel impulse response (CIR) $h_{u,s}(t,\tau)$ can be written as

$$h_{u,s}(t,\tau) = \sum_{l=1}^{L} h_{u,s,l}(t,\tau). \tag{1}$$

The number of clusters is defined as L. t and τ denote the time and delay, respectively. The radio channel of the lth cluster can

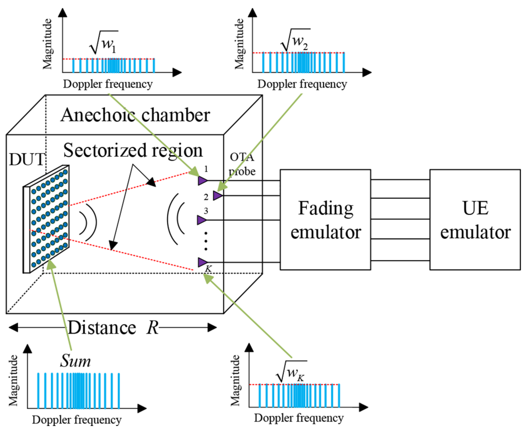

Fig. 2. Diagram of the massive MIMO OTA testing system when implementing the conventional PFS method.

be modelled as [2]

$$h_{u,s,l}(t,\tau) = \sqrt{\frac{P_l}{Q}} \sum_{q=1}^{Q} \begin{bmatrix} F_s^{\mathrm{V}}(\Omega_{l,q}^{\mathrm{AoD}}) \\ F_s^{\mathrm{H}}(\Omega_{l,q}^{\mathrm{AoD}}) \end{bmatrix}^{\mathrm{T}} \begin{bmatrix} \alpha_{l,q}^{\mathrm{VV}} & \alpha_{l,q}^{\mathrm{VH}} \\ \alpha_{l,q}^{\mathrm{HV}} & \alpha_{l,q}^{\mathrm{HH}} \end{bmatrix} \begin{bmatrix} F_u^{\mathrm{V}}(\Omega_{l,q}^{\mathrm{AoA}}) \\ F_u^{\mathrm{H}}(\Omega_{l,q}^{\mathrm{AoA}}) \end{bmatrix} \cdot \exp(j2\pi\nu_{l,q}t) \cdot \exp\left(j\frac{2\pi}{\lambda}\mathbf{r}_{l,q}^{\mathrm{tx}} \cdot \mathbf{d}_s^{\mathrm{tx}}\right) \cdot \exp\left(j\frac{2\pi}{\lambda}\mathbf{r}_{l,q}^{\mathrm{rx}} \cdot \mathbf{d}_u^{\mathrm{rx}}\right) \cdot \delta(\tau-\tau_l). \quad (2)$$

The power and delay of the lth cluster are defined as P_l and τ_l, respectively. The number of rays within a cluster is defined as Q. Here, $F_s^{\mathrm{V}}(\cdot)$ and $F_s^{\mathrm{H}}(\cdot)$ are the vertically and horizontally polarized field patterns of the sth Tx antenna element, respectively. $F_u^{\mathrm{V}}(\cdot)$ and $F_u^{\mathrm{H}}(\cdot)$ are the vertically and horizontally polarized field patterns of the uth Rx antenna element, respectively. $\nu_{l,q}$ represents the Doppler frequency of the qth ray of the lth cluster, and λ is the wavelength. $\Omega_{l,q}^{\mathrm{AoD}}$ and $\Omega_{l,q}^{\mathrm{AoA}}$ are AoD and AoA of the qth ray of the lth cluster, respectively. In addition, the complex amplitude $\alpha_{l,q}^{ab}$ is the independently and identically distributed (i.i.d.) random initial phase for the transmit polarization $a \in [\mathrm{V},\mathrm{H}]$ and the receive polarization $b \in [\mathrm{V},\mathrm{H}]$, which is uniformly distributed over $[0, 2\pi]$. $\mathbf{r}_{l,q}^{\mathrm{rx}}$ and $\mathbf{r}_{l,q}^{\mathrm{tx}}$ are the spherical unit vectors for $\Omega_{l,q}^{\mathrm{AoA}}$ and $\Omega_{l,q}^{\mathrm{AoD}}$, respectively. For the uth Rx antenna, the spatial vector relative to the center of the Rx antenna is $\mathbf{d}_u^{\mathrm{rx}}$. Similarly, the spatial vector of the sth Tx antenna is defined as $\mathbf{d}_s^{\mathrm{tx}}$. Note that the antenna patterns and the phase responses are obtained regarding the center of the Rx panel.

B. Emulated Channel Model Using the Conventional PFS Technique

The MPAC setup for assessing the performance of massive MIMO devices equipped with directional antennas is constructed to study the existing Doppler problem of the current technique. The diagram of the massive MIMO OTA testing system is given in Fig. 2, where the DUT is placed on the Rx side. This setup consists of an anechoic chamber, multiple probe antennas, a probe wall, fading emulators, and user equipment (UE) emulators. Specifically, the anechoic chamber is able to shield interference signals. The probe antennas are placed in appropriate positions on the probe wall. Then, they are connected to the fading emulators. The distance between each active probe and the test area center is defined as R. By considering the Fraunhofer distance [16], [21], assume that the DUT is properly placed in the anechoic chamber to satisfy the far-field condition.

The conventional PFS method is able to synthesize clusters of the target channel using active probe antennas, and each of them has i.i.d. fading channel sequences. Each cluster is mapped to the dual-polarized probe antennas, and the vertical and horizontal polarizations are treated independently and separately. That is, each dual-polarized probe connects to two fading emulator ports by independent feeds. The specific characteristics of clusters, such as delay PSD, cross-polarization power ratio (XPR), spatial-correlation, and Doppler spectrum, are reconstructed in the test area [4], [22], [23].

Following the above procedures, the uplink radio channel environment from the Tx antennas to the Rx antenna array can be emulated in the MPAC setup. The Rx is the DUT, which is placed in the test area, and K probe antennas are used. The channel response $h_{u,s,l}^{\mathrm{PFS,ota}}(t,\tau) \in \mathbb{C}$ for the lth cluster consists of the transfer coefficients from K probe antennas to uth DUT antenna and the fading coefficients of the time-variant CIR, which is defined as $h_{u,s,l}^{\mathrm{PFS,ota}}(t,\tau) = \sum_{k=1}^{K} \exp(j\frac{2\pi}{\lambda}\mathbf{r}_k^{\mathrm{rx}} \cdot \mathbf{d}_u^{\mathrm{rx}}) \cdot \mathbf{F}_u(\Omega_k)^{\mathrm{T}}\mathbf{h}_{k,s,l}^{\mathrm{PFS,ota}}(t,\tau)$. Specifically, the transfer function from the sth Tx antenna to the kth OTA probe for lth cluster consists of some rays, which is written as $\mathbf{h}_{k,s,l}^{\mathrm{PFS,ota}}(t,\tau) = \sqrt{w_k}\sum_{q=1}^{Q} \mathbf{h}_{k,s,l,q}^{\mathrm{ota}}(t,\tau)$. The function $\mathbf{h}_{k,s,l,q}^{\mathrm{ota}}(t,\tau)$ is expressed as

$$\mathbf{h}_{k,s,l,q}^{\mathrm{ota}}(t,\tau) = \sqrt{\frac{P_l}{Q}} \begin{bmatrix} \alpha_{k,l,q}^{\mathrm{VV}} & \alpha_{k,l,q}^{\mathrm{VH}} \\ \alpha_{k,l,q}^{\mathrm{HV}} & \alpha_{k,l,q}^{\mathrm{HH}} \end{bmatrix} \mathbf{F}_s(\Omega_{l,q}^{\mathrm{AoD}}) \cdot \exp(j2\pi\nu_{l,q}t) \cdot \exp\left(j\frac{2\pi}{\lambda}\mathbf{r}_{l,q}^{\mathrm{tx}} \cdot \mathbf{d}_s^{\mathrm{tx}}\right) \cdot \delta(\tau-\tau_l) \quad (3)$$

where w_k denotes the weight of the kth probe when emulating the lth cluster. $\mathbf{F}_u(\Omega_k)$ is the field radiation pattern of the uth Rx antenna for the spatial angle Ω_k of the kth probe, where $\mathbf{F}_u(\Omega_k) = [F_u^{\mathrm{V}}(\Omega_k), F_u^{\mathrm{H}}(\Omega_k)]^{\mathrm{T}}$. $\mathbf{F}_s(\Omega_{l,q}^{\mathrm{AoD}})$ is the field radiation pattern of the sth Tx antenna for the spatial angle $\Omega_{l,q}^{\mathrm{AoD}}$, where $\mathbf{F}_s(\Omega_{l,q}^{\mathrm{AoD}}) = [F_s^{\mathrm{V}}(\Omega_{l,q}^{\mathrm{AoD}}), F_s^{\mathrm{H}}(\Omega_{l,q}^{\mathrm{AoD}})]^{\mathrm{T}}$. After carefully observing $\mathbf{h}_{k,s,l}^{\mathrm{PFS,ota}}(t,\tau)$, the Doppler profiles of different probes are the same when ignoring the impact of the weight w_k. The Doppler spectrum of the cluster around the DUT is synthesized by active probes, as shown in Fig. 2.

Since the Rx equipped with directional antennas will produce different antenna gains for different incoming angles in realistic radio environments, the Doppler spectrum of the emulated channel needs to consider the impact of the Rx radiation pattern in OTA testing. Given that the dependence of the emulated Doppler spectrum on the DUT antenna patterns is ignored for

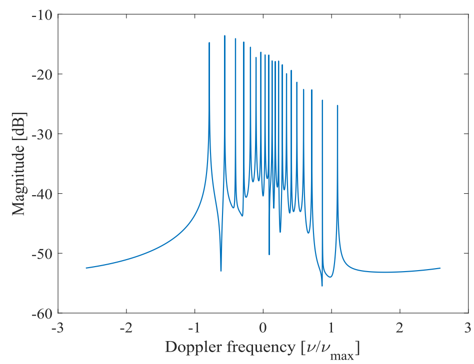

(a)

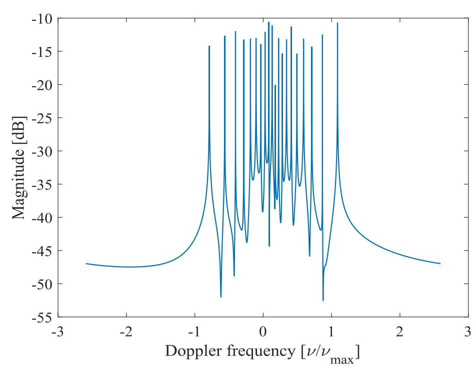

(b)

Fig. 3. Doppler spectrums of cluster #3 shown in Section IV (3 dB beamwidth $= 30^\circ$ and 20 rays within the cluster). (a) Target Doppler spectrum $S(\nu)$. (b) Emulated Doppler spectrum $S^{\mathrm{PFS,ota}}(\nu)$ under the conventional PFS method.

the conventional PFS method, the target Doppler spectrum is not accurately reconstructed if directional-antenna devices are evaluated. For cluster #3 given in Section IV, the Doppler spectrum $S(\nu)$ of the target channel is affected by the Rx antenna element pattern, while the Doppler spectrum $S^{\mathrm{PFS,ota}}(\nu)$ of the emulated channel under the PFS method is unaffected by it, as shown in Fig. 3. This impact depends on the angular PSD of the cluster and the Rx antenna element pattern, especially when the Rx antenna pattern undergoes significant changes in a single cluster. Therefore, improving the accuracy of the emulated Doppler characteristics for measuring directional-antenna devices is one of the focuses of this work.

C. Improved Channel Reconstruction Model

To address the aforementioned problem, an improved channel reconstruction method is proposed, as shown in Fig. 4. For simplicity, only the vertical polarization of the Rx antenna is considered to characterize the Doppler profile for emulation. Using the proposed method, the fading channel sequences between probe antennas are independent of each other and not required the identical distribution. Specifically, the rays within a cluster mapped to each probe are divided into M ray subsets. The power weight $\alpha_{k,m}$ is applied to the mth ray subset of the kth probe, $m = 1, \ldots, M$. Furthermore, the fading channel $\mathbf{h}^{\mathrm{ota}}_{k,s,l}(t,\tau)$ is multiplied by the weight coefficient $\sqrt{w_k}$ and the antenna pattern $\mathbf{F}_u(\Omega_k)$ for the spatial angle Ω_k. Hence, the dependence of the emulated Doppler spectrum on the Rx antenna element pattern can be taken into account by determining the appropriate power weights of the probe antennas and the ray subsets.

Based on the improved channel reconstruction method, the channel emulation model for the lth cluster is modified as

$$\mathbf{h}^{\mathrm{ota}}_{k,s,l}(t,\tau) = \sqrt{w_k}\sum_{m=1}^{M}\sqrt{\alpha_{k,m}}\sum_{q=Q(m-1)/M+1}^{Qm/M}\mathbf{h}^{\mathrm{ota}}_{k,s,l,q}(t,\tau) \tag{4}$$

where $\alpha_{k,m}$ represents the power of the mth ray subset mapped to kth OTA probe. It is clear that the Q rays mapped to each probe are divided into M ray subsets uniformly, and each of them is adjusted by the weight coefficient $\sqrt{\alpha_{k,m}}$.

The CIR $h^{\mathrm{ota}}_{u,s,l}(t,\tau)$ is composed of the transfer vector from K probes to uth Rx antenna and the fading components of the time-variant channel model $\mathbf{h}^{\mathrm{ota}}_{k,s,l}(t,\tau)$, which is defined as

$$h^{\mathrm{ota}}_{u,s,l}(t,\tau) = \sum_{k=1}^{K}\exp\left(j\frac{2\pi}{\lambda}\mathbf{r}^{\mathrm{rx}}_k\cdot\mathbf{d}^{\mathrm{rx}}_u\right)\cdot\mathbf{F}_u(\Omega_k)^{\mathrm{T}}\mathbf{h}^{\mathrm{ota}}_{k,s,l}(t,\tau). \tag{5}$$

In the improved channel emulation model, different power weights $\{\alpha_{k,m}\} \in \mathbb{R}^{K\times M}$ will be allocated separately to the ray subsets, where $\mathbb{R}$ denotes the real number. In OTA testing, the dependence of the Doppler profile on the DUT antenna patterns can be emulated by determining the weights of the probes and ray subsets.

III. Spatial and Temporal Covariance Functions

The covariance function is directly related to the channel characteristics, including the antenna element pattern and the fading distribution of the electromagnetic field [10]. In this section, the covariances of the target channel, the emulated channel using the conventional PFS method, and the improved channel reconstruction model are derived. Firstly, the spatial covariance functions between Rx antennas are explored to characterize the spatial characteristics of the MIMO channel. Secondly, the temporal covariance functions are derived to evaluate their Doppler characteristics. Thirdly, the weight vector $\mathbf{w} = \{w_k\} \in \mathbb{R}^{K\times 1}$ for the active probes and the weight matrix $\mathbf{G} = \{\alpha_{k,m}\} \in \mathbb{R}^{K\times M}$ for the ray subsets are determined by implementing the proposed optimization strategy. Without compromising generality, covariance functions of these three channel models will be calculated based on a single cluster and the vertical polarization case hereafter.

A. Spatial Covariance Functions

1) Target Spatial Covariance: As a statistical measurement, spatial covariance among Rx antennas is studied. By taking (2) into account, the expectation for the product of two rays is zero unless $q = q'$. Assume that the channel is ergodic. For the lth cluster, the spatial covariance between any Rx antenna pair (u_i, u_j) is calculated in the sense of time-averaging

$$R_{u_i,u_j} = \mathbf{E}\{h_{u_i,s,l}(t)\cdot h_{u_j,s,l}(t)^*\}$$

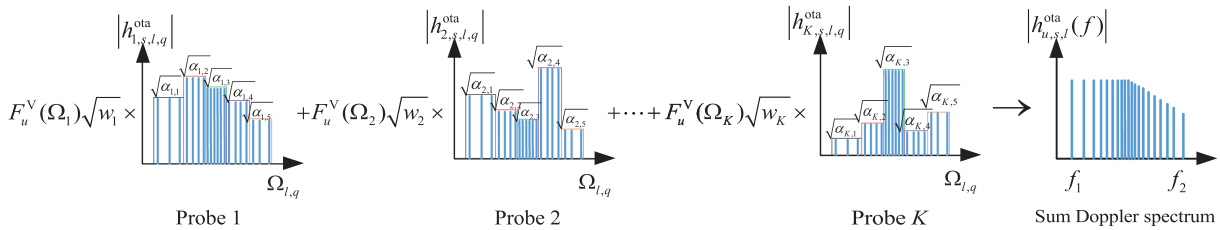

Fig. 4. Diagram of the emulated Doppler profile in OTA testing when applying the improved channel reconstruction method.

$$= P_l \oint F^{\mathrm{V}}_{u_i}(\Omega) \cdot F^{\mathrm{V}}_{u_j}(\Omega)^* \cdot \exp\left(j\frac{2\pi}{\lambda}\mathbf{r}^{\mathrm{rx}}_{l,q} \cdot \mathbf{d}^{\mathrm{rx}}_{u_i}\right) \cdot \exp\left(j\frac{2\pi}{\lambda}\mathbf{r}^{\mathrm{rx}}_{l,q} \cdot \mathbf{d}^{\mathrm{rx}}_{u_j}\right)^* \cdot p(\Omega)d\Omega \quad (6)$$

where $p(\Omega) = p(\phi) \cdot p(\theta)$ denotes the angular PSD of the lth cluster arriving at Rx antennas, and Ω consists of the azimuth angle ϕ and the elevation angle θ. The angular PSD in elevation $p(\theta)$ and the angular PSD in azimuth $p(\phi)$ have a specific shaped distribution, such as the truncated Laplacian distribution. The spatial covariance matrix of the lth cluster can be written as $\mathbf{R} = \{R_{u_i,u_j}\} \in \mathbb{C}^{U\times U}$ when considering all antenna pairs (u_i, u_j) with $i, j = 1, \ldots, U$.

2) Emulated Spatial Covariance Using the Conventional PFS Method: For the lth cluster, the emulated spatial covariance function between any Rx antenna pair (u_i, u_j) using the conventional PFS method is derived as

$$\hat{R}^{\mathrm{PFS,ota}}_{u_i,u_j} = \mathbf{E}\{h^{\mathrm{PFS,ota}}_{u_i,s,l}(t) \cdot h^{\mathrm{PFS,ota}}_{u_j,s,l}(t)^*\} = P_l \sum_{k=1}^{K} F^{\mathrm{V}}_{u_i}(\Omega_k) \cdot F^{\mathrm{V}}_{u_j}(\Omega_k)^* \cdot w_k \cdot \exp\left(j\frac{2\pi}{\lambda}\mathbf{r}^{\mathrm{rx}}_{k} \cdot \mathbf{d}^{\mathrm{rx}}_{u_i}\right) \cdot \exp\left(j\frac{2\pi}{\lambda}\mathbf{r}^{\mathrm{rx}}_{k} \cdot \mathbf{d}^{\mathrm{rx}}_{u_j}\right)^*. \quad (7)$$

For U Rx antennas, the spatial covariance matrix $\hat{\mathbf{R}}^{\mathrm{PFS,ota}}$ of the MIMO channel for emulation can be defined as $\hat{\mathbf{R}}^{\mathrm{PFS,ota}} = \{\hat{R}^{\mathrm{PFS,ota}}_{u_i,u_j}\} \in \mathbb{C}^{U\times U}$, which is affected by the Rx antenna element patterns.

3) Spatial Covariance of the Improved Channel Emulation Model: For the lth cluster, the emulated spatial covariance function between any Rx antenna pair (u_i, u_j) under the improved channel reconstruction model (5) can be derived as

$$\hat{R}^{\mathrm{ota}}_{u_i,u_j} = \mathbf{E}\{h^{\mathrm{ota}}_{u_i,s,l}(t) \cdot h^{\mathrm{ota}}_{u_j,s,l}(t)^*\} = P_l \sum_{k=1}^{K}\sum_{m=1}^{M} F^{\mathrm{V}}_{u_i}(\Omega_k) \cdot F^{\mathrm{V}}_{u_j}(\Omega_k)^* \cdot w_k \cdot \alpha_{k,m} \cdot \frac{Q_m}{Q} \cdot \exp\left(j\frac{2\pi}{\lambda}\mathbf{r}^{\mathrm{rx}}_{k} \cdot \mathbf{d}^{\mathrm{rx}}_{u_i}\right) \cdot \exp\left(j\frac{2\pi}{\lambda}\mathbf{r}^{\mathrm{rx}}_{k} \cdot \mathbf{d}^{\mathrm{rx}}_{u_j}\right)^* \quad (8)$$

where Q_m represents the number of rays for the mth ray subset, and $\sum_{m=1}^{M} Q_m = Q$. Note that the emulated covariance coefficient is a function of the weight w_k and the weight $\alpha_{k,m}$, considering the impact of the Rx antenna pattern. For all Rx antennas, the spatial covariance matrix $\hat{\mathbf{R}}^{\mathrm{ota}}$ for emulation can be written as $\hat{\mathbf{R}}^{\mathrm{ota}} = \{\hat{R}^{\mathrm{ota}}_{u_i,u_j}\} \in \mathbb{C}^{U\times U}$. Similar proofs for the spatial covariances in (6)–(8) are formulated in [17], [22], and thus omitted here.

Constraint 1: Compared with the spatial covariance function in (7), the covariance function between Rx antennas in (8) is affected not only by the probe weight vector $\mathbf{w}$ but also by the weight matrix $\mathbf{G}$ of the ray subset. However, the spatial covariance function in (8) will equal the covariance function in (7) if the condition $\sum_{m=1}^{M} \alpha_{k,m} \cdot \frac{Q_m}{Q} = 1$ for an arbitrary kth probe can be satisfied. The constraint condition will show significant bearing on the optimization algorithm design proposed in this article, which will be explained in detail later.

B. Temporal Covariance Functions

1) Target Temporal Covariance: In wireless communications, the motion speed and the direction of the UE terminal result in the Doppler effect to produce the frequency spread of the received signals. Since the Doppler PSD is a Fourier transform pair with the temporal-correlation function [20], the temporal covariance function will be derived to describe the Doppler characteristics of the MIMO channels in this sub-section. In view of the target radio channel in (2), the temporal covariance coefficient of an arbitrary time pair (t_1, t_n) on the uth Rx antenna, $n = 1, \ldots, N$, is derived as

$$R_u(t_1, t_n) = \mathbf{E}\{h_{u,s,l}(t_1) \cdot h_{u,s,l}(t_n)^*\} = \frac{P_l}{Q}\sum_{q=1}^{Q} F^{\mathrm{V}}_{u}(\Omega^{\mathrm{AoA}}_{l,q}) \cdot F^{\mathrm{V}}_{u}(\Omega^{\mathrm{AoA}}_{l,q})^* \cdot \exp(j2\pi\nu_{l,q}t_1) \cdot \exp(j2\pi\nu_{l,q}t_n)^*. \quad (9)$$

2) Emulated Temporal Covariance Using the Conventional PFS Method: Similar to the temporal covariance under the target channel, the temporal covariance coefficient of the emulated channel $h^{\mathrm{PFS,ota}}_{u,s,l}(t,\tau)$ for an arbitrary time pair (t_1, t_n) can be described as

$$\hat{R}^{\mathrm{PFS,ota}}_{u}(t_1, t_n) = \mathbf{E}\{h^{\mathrm{PFS,ota}}_{u,s,l}(t_1) \cdot h^{\mathrm{PFS,ota}}_{u,s,l}(t_n)^*\} = \sum_{k=1}^{K} F^{\mathrm{V}}_{u}(\Omega_k) \cdot F^{\mathrm{V}}_{u}(\Omega_k)^* \cdot w_k \cdot \frac{P_l}{Q} \sum_{q=1}^{Q} \exp(j2\pi\nu_{l,q}t_1) \cdot \exp(j2\pi\nu_{l,q}t_n)^*. \quad (10)$$

3) Temporal Covariance of the Improved Channel Emulation Model: The temporal covariance coefficient of the improved channel reconstruction model $h_{u,s,l}^{\text{ota}}(t,\tau)$ for an arbitrary time pair (t_1, t_n) can be described as

$$\begin{aligned}\hat{R}_u^{\text{ota}}(t_1,t_n) &= \mathbf{E}\{h_{u,s,l}^{\text{ota}}(t_1)\cdot h_{u,s,l}^{\text{ota}}(t_n)^*\}\\ &= \sum_{k=1}^{K} F_u^{\text{V}}(\Omega_k)\cdot F_u^{\text{V}}(\Omega_k)^*\cdot w_k\cdot \frac{P_l}{Q}\cdot \sum_{m=1}^{M}\alpha_{k,m}\\ &\sum_{q=Q(m-1)/m+1}^{Qm/M} \exp(j2\pi\nu_{l,q}t_1)\cdot \exp(j2\pi\nu_{l,q}t_n)^*. \end{aligned} \tag{11}$$

Similar proofs for the temporal covariances in (9)–(11) are also formulated in [17], [22], and thus omitted here.

Constraint 2: Compared to (10), the weight matrix $\mathbf{G} = \{\alpha_{k,m}\} \in \mathbb{R}^{K\times M}$ is allocated to adjust the Doppler profile mapped to each probe when using the improved channel emulation model in (11). According to the antenna element pattern of the DUT, the weight $\alpha_{k,m}$ of each ray subset can be appropriately adjusted to guarantee the dependence of the emulated Doppler spectrum on the Rx antenna pattern. In summary, active probe antennas will have different Doppler information by changing the ray subset weights mapped to each probe for the improved channel reconstruction method. Following the above statements, it is clear that the more ray subsets are allocated for each probe, the more accurate the dependence of the Doppler spectrum on impinging ray angles will be, especially when the number of the ray subsets M equals Q. This inference will be further verified in the validation section.

C. Optimal Weights

Both the spatial covariance function and the temporal covariance function of the improved channel emulation model have been derived. Next, the core of reconstructing the target channel is to obtain the unknown weights of the improved model accurately. In (8) and (11), the weight vector $\mathbf{w} = \{w_k\} \in \mathbb{R}^{K\times 1}$ and the weight matrix $\mathbf{G} = \{\alpha_{k,m}\} \in \mathbb{R}^{K\times M}$ need to be allocated to reconstruct the target channel as accurately as possible. Compared with existing works that use the spatial-correlation function to assess the performance of the emulated channel [4], [5], [24], the joint optimization between the spatial characteristics and the Doppler characteristics is required to determine the optimal weight vector $\mathbf{w}$ and weight matrix $\mathbf{G}$. But optimizing the temporal covariance deviation function and the spatial covariance deviation function at the same time will limit the improvement of the reconstructed Doppler profile in the test area. Inspired by the above statements, a novel optimization strategy considering the constraint in *constraint 1* is proposed to determine the weight vector $\mathbf{w}$ and the weight matrix $\mathbf{G}$ as follows.

Specifically, the proposed optimization strategy will not degrade the accuracy of the spatial-correlation of the emulated channel. The power weight $\mathbf{w}$ can be directly obtained by optimizing the spatial covariance deviation function between (6) and (7), regardless of ray subsets of probes. Then, the deviation function of the temporal covariance is established as a metric to assess the Doppler characteristics of the improved channel reconstruction model. The constraint condition mentioned in *constraint 1* is considered when optimizing the temporal covariance deviation function to determine the unknown matrix $\mathbf{G}$. The detailed calculation processes for the weight vector $\mathbf{w}$ and the weight matrix $\mathbf{G}$ are described in detail below.

Step 1: The deviation function between the matrix $\mathbf{R}$ and the matrix $\hat{\mathbf{R}}^{\text{ota}}(\mathbf{G},\mathbf{w})$ can be written as the Frobenius norm to minimize for all Rx antenna pairs. Therefore, the weight vector $\mathbf{w}$ of the improved channel reconstruction model can be determined

$$\begin{aligned}&\underset{\mathbf{w}}{\text{minimize}}\ \|\mathbf{R}-\hat{\mathbf{R}}^{\text{ota}}(\mathbf{G},\mathbf{w})\|_2^2\\ &\text{s.t.}\quad \mathbf{G}\xi = \boldsymbol{\eta},\quad \|\mathbf{w}\|_1 = 1,\\ &\qquad \mathbf{G}\geq 0,\quad 0\leq w_k\leq 1\end{aligned} \tag{12}$$

where $\xi = [\frac{Q_1}{Q}, \frac{Q_2}{Q}, \ldots, \frac{Q_M}{Q}]^T \in \mathbb{R}^{M\times 1}$ and $\boldsymbol{\eta} = [1, 1, \ldots, 1]^T \in \mathbb{R}^{K\times 1}$. Each element of the matrix $\mathbf{G}$ is not less than 0 for $\mathbf{G} \geq 0$. In view of the *constraint 1*, (12) can be reduced to (13) when considering the constraint condition $\sum_{m=1}^{M} \alpha_{k,m}\cdot \frac{Q_m}{Q} = 1$ for K active probes

$$\begin{aligned}\iff\quad &\underset{\mathbf{w}}{\text{minimize}}\ \|\mathbf{R}-\hat{\mathbf{R}}^{\text{PFS,ota}}(\mathbf{w})\|_2^2\\ &\text{s.t.}\quad \|\mathbf{w}\|_1 = 1,\quad 0\leq w_k\leq 1.\end{aligned} \tag{13}$$

Step 2: Substituting the obtained weight vector $\mathbf{w}$ into (11), the deviation function between the temporal covariance $R_u(t_1,t_n)$ and the temporal covariance $\hat{R}_u^{\text{ota}}(t_1,t_n;\mathbf{G})$ is also described in the Frobenius norm. It is further minimized for all sample time pairs (t_1,t_n) at the uth Rx antenna. Therefore, the weight matrix $\mathbf{G}$ of the improved channel emulation model can be determined

$$\begin{aligned}&\underset{\mathbf{G}}{\text{minimize}}\ \|R_u(t_1,t_n)-\hat{R}_u^{\text{ota}}(t_1,t_n;\mathbf{G})\|_2^2\\ &\text{s.t.}\quad \mathbf{G}\xi = \boldsymbol{\eta},\quad \mathbf{G}\geq 0.\end{aligned} \tag{14}$$

Using the constraint $\mathbf{G}\xi = \boldsymbol{\eta}$, the proposed optimization strategy is to improve the accuracy of the reconstructed temporal covariances without compromising the emulated spatial covariances. (8) can be simplified to (7). This means that the ray allocation can be ignored when performing the proposed optimization strategy to determine the probe weight $\mathbf{w}$. This is simple and valid for determining unknown parameters. Incidentally, (13) and (14) are convex programming problems even if the linear constraints are taken into account, and the results can be easily obtained.

IV. Validation and Discussion

A. Simulation Scenarios

In order to validate the existing Doppler defect of the reconstructed channel under the conventional PFS method when

TABLE I
SIMULATION SCENARIOS

Cluster	Cluster center	Velocity (km/h)	Rx antenna 3dB beamwidth
Cluster #1	AoA = 9.3° EoA = -15.8°	100	30°, 65°, 90°, 360°
Cluster #2	AoA = -11.4° EoA = -13.2°	100	30°, 65°, 90°, 360°
Cluster #3	AoA = 30.6° EoA = -13°	100	30°, 65°, 90°, 360°
Cluster #4	AoA = -34.1° EoA = -25.3°	100	30°, 65°, 90°, 360°

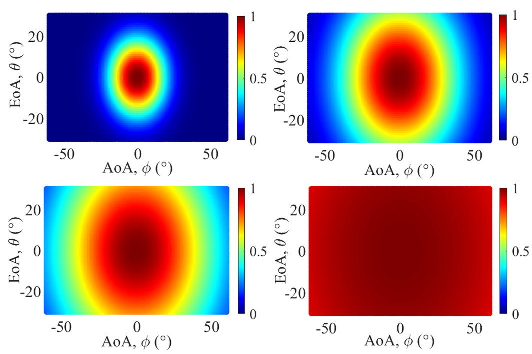

Fig. 5. Radiation patterns of the Rx antenna elements in the angle area of probe wall. (a) 3 dB beamwidth = 30°. (b) 3 dB beamwidth = 65°. (c) 3 dB beamwidth = 90°. (d) Omni-directional antenna.

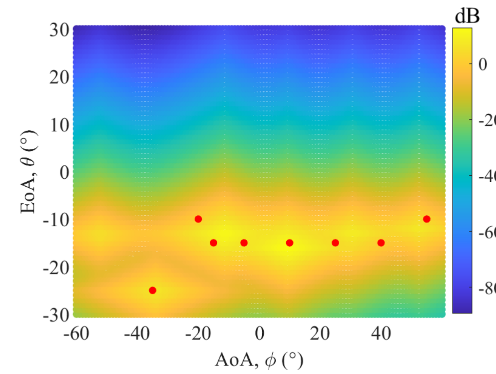

Fig. 6. Target angular PSD of the CDL-B model and 8 active probe antennas.

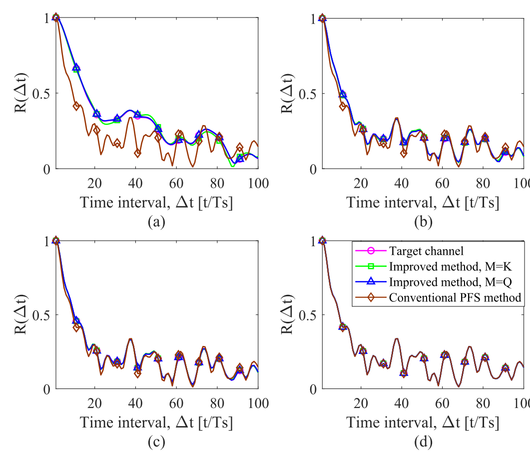

Fig. 7. Temporal correlations of the reconstructed channels and the target channel for cluster #1. (a) 3 dB beamwidth = 30°. (b) 3 dB beamwidth = 65°. (c) 3 dB beamwidth = 90°. (d) Omni-directional antenna.

measuring directional-antenna devices and verify the link performance of the improved reconstruction channel, various simulations with an operating frequency of 28 GHz are given in Table I. There is an ideal dipole antenna on the Tx side. On the Rx side, the massive MIMO BSs with different directional antenna elements are placed in the test area as the DUT, and the probe antennas are located in the far-field radiated by the DUT. The antennas are vertically polarized. In the uplink, the Rx antenna array is composed of 8×8 directional antennas with the element spacing of 0.5λ. The maximal separation of this array is $3.5\times\sqrt{2}\lambda$. The Rx antenna element pattern specified by the 3GPP TR 38.901 standard is used as an example in simulations. The mutual coupling among antenna elements is omitted, and the radiation pattern is assumed to be the same for each antenna element. In Table I, the 3 dB beamwidths of the Rx antennas are 30°, 65°, 90°, and 360°. The velocity of the Tx terminal is $v =$ 100 km/h, and its direction is [0,1,0] with reference to the center of the Rx panel.

In the probe wall area, Fig. 5 shows the radiation patterns of different directional antennas and the omni-directional antenna. Obviously, the antenna pattern gains of the directional Rx antenna are different, while the pattern gains of the omni-directional antenna are close to 1. 6 clusters with high power are considered (see CDL-B model in [2]), and the center angles of them are (9.3°, −15.8°), (−11.4°, −13.2°), (30.6°, −13°), (−34.1°, −25.3°), (52.5°, −13.2°), and (−52.2°, −12°). By the way, the total power of the clusters is set to 1. ASA and ESA are 10° and 3°, respectively. There are 20 rays in a cluster, $Q = 20$. Considering all clusters, the multi-shot algorithm based on spatial-correlation metric is carried out [7]. Then, 8 active probes are obtained, which are marked with red points in Fig. 6. The cluster-based channel model is a GBSM in [3], which is adopted in MIMO OTA standards.

B. Temporal Correlation

Simulation results for temporal correlation functions are given to validate the Doppler profile of the improved channel emulation model for different scenarios. In Figs. 7–10, the temporal correlations of clusters #1–4 are shown. There are 100 time sampling points, where $\Delta t = 1, \ldots, 100$, and the sampling interval is normalized to sampling time T_s. To study the influence of the DUT antenna pattern on the emulated temporal correlation, different antenna element patterns are simulated for each cluster. Firstly, there exist inaccurate temporal correlations for emulation when performing the conventional PFS method to assess the performance of the directional-antenna devices. Obviously, the stronger the directivity of the antenna element is, the more pronounced the problem displayed will be. Secondly, the favorable performance of the proposed method is examined from two perspectives. The number of ray subsets M mapped to each probe equals the number of probes K and the number of rays Q. $M = K$ means that 20 rays mapped to every probe are

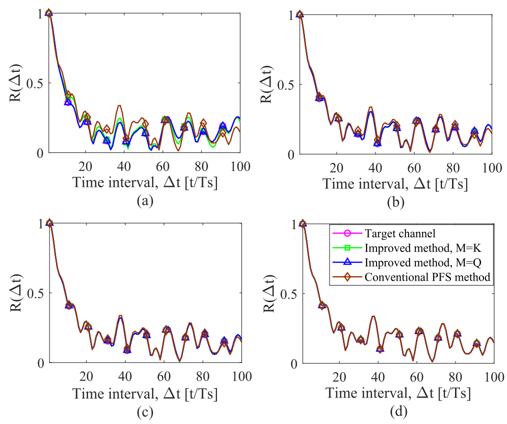

Fig. 8. Temporal correlations of the reconstructed channels and the target channel for cluster #2. (a) 3 dB beamwidth = 30°. (b) 3 dB beamwidth = 65°. (c) 3 dB beamwidth = 90°. (d) Omni-directional antenna.

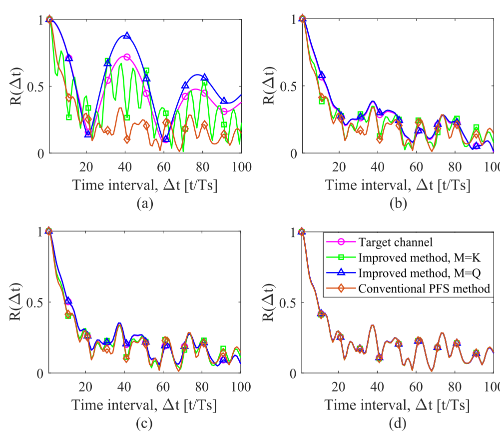

Fig. 9. Temporal correlations of the reconstructed channels and the target channel for cluster #3. (a) 3 dB beamwidth = 30°. (b) 3 dB beamwidth = 65°. (c) 3 dB beamwidth = 90°. (d) Omni-directional antenna.

divided into 8 ray subsets, each of which separately includes 2, 2, 2, 2, 3, 3, 3, and 3 rays. Therefore, 8×8 ray subset weights need to be determined. $M = Q$ means that 20 rays mapped to every probe are divided into 20 ray subsets. That is, the rays within a cluster are weighted separately, and 8×20 ray subset weights need to be allocated.

Unlike the conventional PFS method for channel emulation, the improved channel reconstruction model can emulate the target Doppler profile more accurately when measuring directional-antenna devices. The accuracy of the reconstructed temporal correlations increases under the more subset weights. That is, the more the number of ray subsets allocated, the more accurate the dependence of the Doppler spectrum on impinging ray angles. In addition, available simulation results for omni-directional antenna devices are compared with those of directional-antenna devices. For measuring omni-directional antenna devices, the emulated temporal correlations for different clusters are shown in the fourth sub-figures of Figs. 7–10. This confirms the fact that the current PFS method is capable of reconstructing the target Doppler spectrum when the DUT antenna elements are

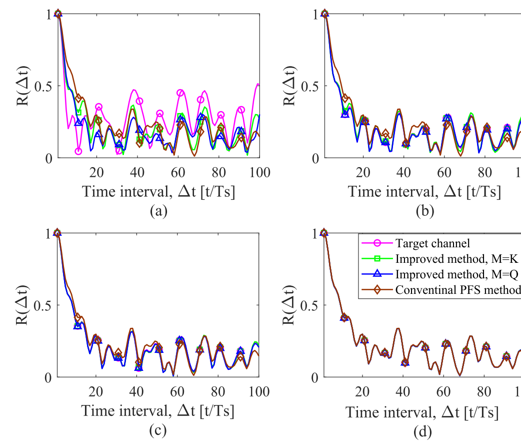

Fig. 10. Temporal correlations of the reconstructed channels and the target channel for cluster #4. (a) 3 dB beamwidth = 30°. (b) 3 dB beamwidth = 65°. (c) 3 dB beamwidth = 90°. (d) Omni-directional antenna.

TABLE II
RMSEs OF THE EMULATED TEMPORAL CORRELATIONS IN (15)

Clusters		Rx antenna 3dB beamwidth			
		30°	65°	90°	360°
1	PFS	0.1284	0.0371	0.0203	0.0013
	M = K	0.0144	0.0042	0.0022	1.4×10^{-4}
	M = Q	0.0030	9.5×10^{-4}	2.0×10^{-4}	3.7×10^{-5}
2	PFS	0.0610	0.0190	0.0105	7.0×10^{-4}
	M = K	0.0224	0.0018	0.0013	1.4×10^{-4}
	M = Q	0.0083	0.0014	0.0012	1.1×10^{-4}
3	PFS	0.2783	0.0836	0.0458	0.0030
	M = K	0.1793	0.0096	0.0047	3.9×10^{-4}
	M = Q	0.0895	0.0067	0.0023	7.5×10^{-5}
4	PFS	0.1739	0.0525	0.0307	0.0022
	M = K	0.1477	0.0116	0.0039	2.34×10^{-4}
	M = Q	0.1364	0.0068	0.0030	2.13×10^{-4}

omni-directional. Note that the improvement on Doppler emulation by using the proposed method is not obvious when the DUT antenna element is not very directive. In summary, the proposed channel emulation method is not only able to assess the performance of omni-directional antenna devices, but also evaluate that of directional-antenna devices based on the DUT antenna element patterns.

The root-mean-square error (RMSE) of the channel emulation over the whole time delay of interest is defined as the root-mean-square of the differences in linear scale between the emulated temporal correlations and the target temporal correlations, which is given by

$$RMSE = \sqrt{\frac{1}{N}\|R_u(\Delta t) - \hat{R}_u^{\text{ota}}(\Delta t)\|_2^2}. \tag{15}$$

Based on (15), the RMSEs of the temporal correlations for different clusters are calculated in Table II. We can obtain the same conclusions through numerical analysis. It is clear that the RMSE gradually decreases as the Rx antenna 3 dB beamwidth increases. The proposed channel reconstruction method is superior to the conventional PFS technique when assessing the performance of directional-antenna devices in the MPAC setup.

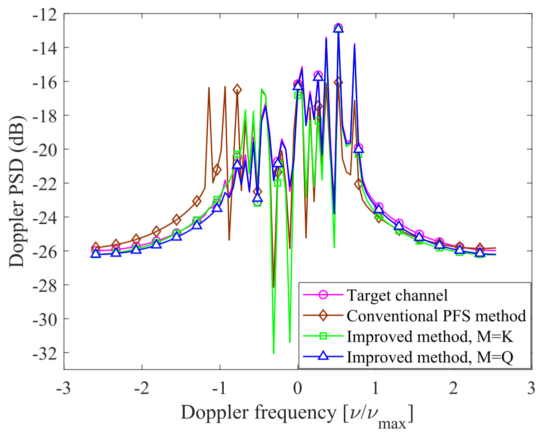

Fig. 11. Doppler PSDs of the reconstructed channels and the target channel for cluster #3 under the Rx antenna 3 dB beamwidths = 30°.

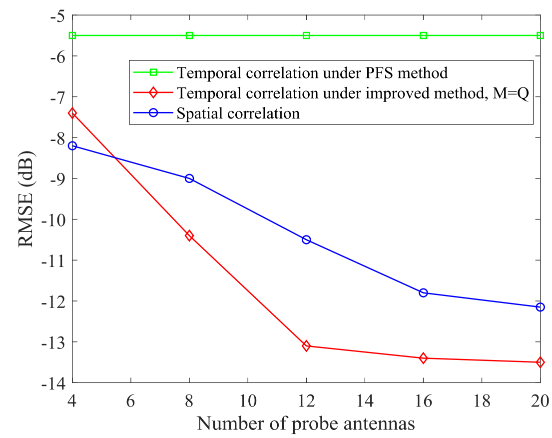

Fig. 12. RMSEs of the emulated temporal correlations and spatial correlations as a function of the number of OTA probes for cluster #3 under the Rx antenna 3 dB beamwidths = 30°.

C. Doppler PSD

Performing Fourier transforms on (9)–(11), the Doppler PSDs of the reconstructed channels and target channel are obtained for cluster #3 under the Rx antenna 3 dB beamwidth = 30°, which are shown in Fig. 11. The purple curve represents the target Doppler PSD, and the red curve represents the emulated Doppler PSD using the conventional PFS method. There is the Doppler defect used to assess the performance of directional-antenna devices, and the RMSE is −22.3 dB. Hence, the reconstructed channel cannot accurately emulate Doppler characteristics of the realistic radio link. This means that the link performance of the DUT cannot be accurately evaluated in the MPAC setup. The green curve describes the Doppler PSD of the improved channel emulation model with $M = K$, and the blue curve describes the Doppler PSD of the improved channel emulation model with $M = Q$. The RMSEs of these two curves are −24.9 dB and −29.2 dB. These results also show that the proposed channel emulation method is more accurate than the conventional PFS method for reconstructing the Doppler profile of the target channel. Moreover, the proposed optimization strategy is also effective. Compared with $M = K$, the Doppler PSD for emulation can be performed better around directional-antenna devices under $M = Q$.

D. Impacts of the Number of Probes and the Number of Rays Within a Cluster on the Emulated Temporal Correlations

To fully study the performance of the proposed method, this section explores the impact of the number of active probes on the Doppler profile of the emulated channels. In Fig. 12, the RMSEs of the reconstructed correlations as a function of the number of active probes are shown for cluster #3 under the Rx antenna 3 dB beamwidths = 30°. 4, 8, 12, 16, and 20 optimal probes are selected in turn. Firstly, the blue curve describes the RMSE of the reconstructed spatial correlation, which gradually reduces with increasing probe antennas under the given test area. Secondly, the green curve shows the relationship between the number of active probes and the emulated temporal correlation under the conventional PFS method. There is a fixed RMSE of −5.5 dB between the reconstructed temporal correlation and the target one. This means that the number of active probes will not affect the RMSE under the PFS method, as the i.i.d. channel sequences are mapped to probes when synthesizing clusters. Thirdly, the red curve describes the impact of the number of active probes on the RMSE of the reconstructed temporal correlation under the improved channel emulation method, $M = Q$. The RMSE of the reconstructed temporal correlation is smaller than that of the current PFS method, and the error decreases with increasing the number of active probes due to increasing the unknown weight freedom. However, it is hardly affected when the number of active probes is large. The reason for this is that the additional constraint mentioned in *constraint 1*, $\sum_{m=1}^{M} \alpha_{k,m} \cdot \frac{Q_m}{Q} = 1$ for every probe, is considered to ensure the accuracy of the reconstructed spatial characteristics. The number of constraint conditions increases with increasing the number of OTA probes, which limits the improvement on the emulated Doppler profile. However, to increase the accuracy of the spatial characteristics of the emulated channel, it is crucial to increase the number of active probes.

Following the above discussions, separately adjusting each ray weight mapped to probes, $M = Q$, can significantly improve the accuracy of the emulated Doppler profile when measuring the performance of the directional-antenna devices in OTA testing. Naturally, it is valuable to investigate the impact of the number of rays within a cluster on the reconstructed temporal correlation. Fig. 13 shows the RMSE of the reconstructed temporal correlation as a function of the number of rays for cluster #3 under different methods. The RMSE is hardly affected by the number of rays within clusters, especially when the number of rays is large. The reason is that the proposed channel emulation method tends to recreate the Doppler component of each ray by adding appropriate weights. Obviously, this method is able to guarantee the dependence of the Doppler spectrum on impinging ray angles. The ray weights will have more freedom when increasing the number of rays Q under the constraint $\sum_{m=1}^{Q} \alpha_{k,m} = Q$. But, the target channel will have more Doppler components to be emulated. That is, the more ray weights $\{\alpha_{k,m}\} \in \mathbb{R}^{K\times M}$

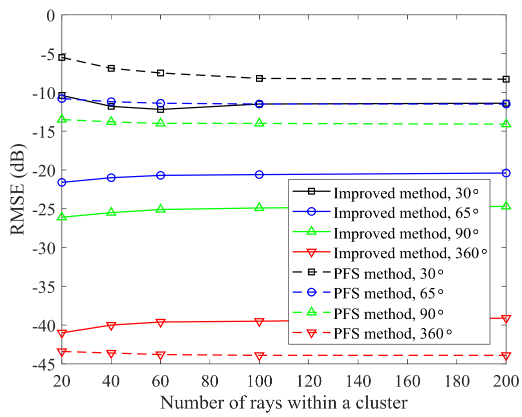

Fig. 13. RMSEs of the emulated temporal correlations as a function of the number of rays for cluster #3.

need to be adjusted for the improved channel reconstruction method. However, it is also important to increase the number of rays within a cluster, as it ensures independence among active probes.

E. Implementation and Feasibility

Following mentioned above, the improved channel emulation method can synthesize any type of fading channel sequences in the MPAC setups, which is similar to the current PFS technique. However, the difference is that the proposed model only ensures the independence of the fading channel sequences mapped to active probes without retaining the identical distribution of these fading sequences. But the implementation of the improved technique is the same as that of the traditional PFS method and does not require additional hardware resources in a practical or operational context.

In current MIMO OTA tests, the DUT antenna patterns are usually assumed to be omni-directional, especially in FR1. The DUT antenna element patterns are not required to measure in compliance tests. However, the DUT may be equipped with directional antenna elements. It is inaccurate to perform MIMO OTA testing if the DUT is regarded as a "black box" without exact information about its antennas. In summary, the DUT antenna pattern is significant for generating the fading sequences to measure the performance of directional-antenna devices, which is similar to the radiated two-stage (RTS) method [25]. The antenna element pattern of the DUT can be measured, and the specific steps are described below.

1) In an anechoic chamber, place two calibration antennas with omni-directional radiation patterns within the azimuth and elevation ranges vertically and horizontally in the test area, and then obtain the radio path loss of the test system at a specific frequency.

2) Remove the calibration antennas and place the DUT in the center of the test area. The DUT antenna element and probe antenna are connected to a vector network analyzer (VNA). Any one element of the DUT antenna array is selectively fed, while other elements are terminated. The DUT is rotated by the turntable to sample in the angular domain, and then the S-parameters between the antenna element and the probe are measured at different angles. Hence, the signal level matrix for all antenna elements received by VNA is recorded from simultaneous excitation. This matrix includes the magnitude and phase information, and the complex radiation patterns of the antenna elements are measured after compensating for the radio path loss.

Similar to existing massive MIMO OTA testing, e.g., [14], [15], [16], [17], [19], the mutual coupling among antenna elements is ignored in the simulations. The directivity of every antenna element for the DUT is assumed to be the same. In practice, the radiation patterns between antenna elements may be different due to the impact of mutual coupling. An interesting topic for future work is to research the impact of mutual coupling among antennas on the proposed channel emulation method.

V. Conclusion

This article has demonstrated that the conventional PFS method cannot be used to accurately create the Doppler characteristics of the realistic radio channels when measuring the performance of directional-antenna devices in the MPAC setup, as it ignores the influence of DUT antenna element patterns on the emulated Doppler spectrum. This impact depends on the angular PSD of the cluster and the antenna element pattern of the DUT, especially when the DUT antenna pattern changes severely for a cluster. Therefore, an improved channel emulation model has been proposed to solve the shortcoming of the conventional PFS method considering the measured DUT antenna element patterns. The rays within a cluster mapped to each probe have been divided into multiple subsets, and each subset has been weighted. Furthermore, the temporal covariance deviation function between the target channel and the reconstructed channel has been established to determine the ray subset weights when considering the constraints. Simulations of the temporal correlation have been given to verify the effectiveness of the proposed channel model for emulation under various scenarios. Results have shown that this method can address the existing Doppler defect of the emulated channel without degrading its spatial properties when assessing directional-antenna devices in the MPAC setups. The greater the number of ray subsets for probes is, the more pronounced the performance of the proposed method will be. Moreover, the Doppler profile of the proposed channel emulation model is almost unaffected by the number of rays within the clusters.

References

[1] 3rd Generation Partnership Project, "Verification of radiated multi-antenna reception performance of user equipment," 3GPP, Sophia Antipolis, France, Tech. Rep. 37.977, Sep. 2013.

[2] 3rd Generation Partnership Project, "Study on channel model for frequencies from 0.5 to 100 GHz," 3GPP, Sophia Antipolis, France, Tech. Rep. 38.901, Jul. 2017.

[3] P. Kyösti et al., "WINNER II channel models, deliverable 1.1.2. v1.2, IST-4-027756 WINNER II," Tech. Rep., Sep. 2007.

[4] P. Kyösti, T. Jämsä, and J. Nuutinen, "Channel modelling for multi-probe over-the-air MIMO testing," *Int. J. Antennas Propag.*, vol. 2012, pp. 1–11, Mar. 2012.

[5] W. Fan, X. C. B. Lisbona, F. Sun, J.Ø. Nielsen, M. B. Knudsen, and G. F. Pedersen, "Emulating spatial characteristics of MIMO channels for OTA testing," *IEEE Trans. Antennas Propag.*, vol. 61, no. 8, pp. 4306–4314, Aug. 2013.

[6] A. Khatun, T. Laitinen, V. Kolmonen, and P. Vainikainen, "Dependence of error level on the number of probes in over-the-air multiprobe test systems," *Int. J. Antennas Propag.*, vol. 2012, pp. 1–6, May 2012.

[7] W. Fan et al., "Probe selection in multiprobe OTA setups," *IEEE Trans. Antennas Propag.*, vol. 62, no. 4, pp. 2109–2120, Apr. 2014.

[8] M. Pätzold, "System function and characteristic quantities of spatial deterministic Gaussian uncorrelated scattering processes," in *Proc. 57th IEEE Veh. Technol. Conf.*, 2003, pp. 256–261.

[9] M. Pätzold, B. O. Hogstad, and N. Youssef, "Modeling, analysis, and simulation of MIMO mobile-to-mobile fading channels," *IEEE Trans. Wireless Commun.*, vol. 7, no. 2, pp. 510–520, Feb. 2008.

[10] E. Tsakalaki, O. N. Alrabadi, W. Fan, and G. F. Pedersen, "Covariance-based spatial channel structure emulation for MIMO OTA testing," *IEEE Commun. Lett.*, vol. 18, no. 2, pp. 205–208, Feb. 2014.

[11] W. Fan et al., "Antenna pattern impact on MIMO OTA testing," *IEEE Trans. Antennas Propag.*, vol. 61, no. 11, pp. 5714–5723, Nov. 2013.

[12] L. Xin, Y. Li, S. Zhe, and X. Zhang, "On over-the-air testing for devices with directional antennas," *IEEE Access*, vol. 8, pp. 121821–121832, Jul. 2020.

[13] E. G. Larsson, O. Edfors, F. Tufvesson, and T. Marzetta, "Massive MIMO for next generation wireless systems," *IEEE Commun. Mag.*, vol. 52, no. 2, pp. 186–195, Feb. 2014.

[14] P. Kyösti, L. Hentilä, W. Fan, J. Lehtomäki, and M. Latva-Aho, "On radiated performance evaluation of massive MIMO devices in multiprobe anechoic chamber OTA setups," *IEEE Trans. Antennas Propag.*, vol. 66, no. 10, pp. 5485–5497, Oct. 2018.

[15] W. Fan et al., "A step toward 5G in 2020: Low-cost OTA performance evaluation of massive MIMO base stations," *IEEE Antennas Propag. Mag.*, vol. 59, no. 1, pp. 38–47, Feb. 2017.

[16] P. Kyösti, W. Fan, G. F. Pedersen, and M. Latva-Aho, "On dimensions of OTA setups for massive MIMO base stations radiated testing," *IEEE Access*, vol. 4, pp. 5971–5981, 2016.

[17] L. Xin, Y. Li, H. Sun, and G. Wei, "A non-Kronecker structured PFS method for channel emulation in multiprobe OTA setups," *IEEE Trans. Antennas Propag.*, vol. 71, no. 6, pp. 5349–5360, Jun. 2023.

[18] Y. Li, L. Xin, X. Liu, and X. Zhang, "Dual anechoic chamber setup for over-the-air radiated testing of 5G devices," *IEEE Trans. Antennas Propag.*, vol. 68, no. 3, pp. 2469–2474, Mar. 2020.

[19] Y. Li, L. Xin, and X. Zhang, "On probe weighting for massive MIMO OTA testing based on angular spectrum similarity," *IEEE Antennas Wireless Propag. Lett.*, vol. 18, no. 7, pp. 1497–1501, Jul. 2019.

[20] B. H. Fleury, "First- and second-order characterization of direction dispersion and space selectivity in the radio channel," *IEEE Trans. Inf. Theory*, vol. 46, no. 6, pp. 2027–2044, Sep. 2000.

[21] "Test plan for wireless device over-the-air performance: Method of measurement for radiated RF power and receiver performance," CTIA Certification, Tech. Rep. Version 3.5.2, Sep. 2015.

[22] Y. Ji, W. Fan, G. F. Pedersen, and X. Wu, "On channel emulation methods in multiprobe anechoic chamber setups for over-the-air testing," *IEEE Trans. Veh. Technol.*, vol. 67, no. 8, pp. 6740–6751, Aug. 2018.

[23] W. Fan, L. Hentilä, P. Kyösti, and G. F. Pedersen, "Test zone size characterization with measured MIMO throughput for simulated MPAC configurations in conductive setups," *IEEE Trans. Veh. Technol.*, vol. 66, no. 11, pp. 10532–10536, Nov. 2017.

[24] M. A. Mow, B. Niu, R. W. Schlub, and R. Caballero, "Tools for design and analysis of over-the-air test systems with channel model emulation capabilities," US patent 2011/0270567, 2011.

[25] Y. Jing, H. Kong, and M. Rumney, "MIMO OTA test for a mobile station performance evaluation," *IEEE Instrument. Meas. Mag.*, vol. 19, no. 3, pp. 43–50, Jun. 2016.

Lijian Xin (Member, IEEE) received the Ph.D. degree in information and communications engineering from Beijing University of Posts and Telecommunications, Beijing, China, in 2021. He is currently with Purple Mountain Laboratories as an Assistant Research Fellow, Nanjing, China. His research interests include over-the-air testing of massive MIMO devices, channel measurement, and modeling.

Yong Li (Member, IEEE) received the Ph.D. degree in signal and information processing from Beijing University of Posts and Telecommunications (BUPT), Beijing, China in 2009. He is a Full Professor with the School of Information and Communication Engineering, BUPT. His research interests include over-the-air testing, space-air-ground integrated network, and beyond-5G system. He has published more than 100 papers in journals, conference proceedings and workshops, and filed more than 60 patents. He was the recipient of the First Grade Award of the Technological Invention from China Institute of Communications.

Cheng-Xiang Wang (Fellow, IEEE) received the B.Sc. and M.Eng. degrees in communication and information systems from Shandong University, Jinan, China, in 1997 and 2000, respectively, and the Ph.D. degree in wireless communications from Aalborg University, Aalborg, Denmark, in 2004. He was a Research Assistant with the Hamburg University of Technology, Hamburg, Germany, from 2000 to 2001, Visiting Researcher with Siemens AG Mobile Phones, Munich, Germany, in 2004, and Research Fellow with the University of Agder, Grimstad, Norway, from 2001 to 2005. Since 2005, he has been with Heriot-Watt University, Edinburgh, U.K., where he was promoted to a Professor in 2011. In 2018, he was with Southeast University, Nanjing, China, as a Professor. He is also a part-time Professor with Purple Mountain Laboratories, Nanjing. He has authored 4 books, 3 book chapters, and more than 500 papers in refereed journals and conference proceedings, including 27 highly cited papers. He has also delivered 24 invited keynote speeches/talks and 16 tutorials in international conferences. His research interests include wireless channel measurements and modeling, 6G wireless communication networks, and electromagnetic information theory. Dr. Wang is a Member of the Academia Europaea (The Academy of Europe) and European Academy of Sciences and Arts, the Fellow of the Royal Society of Edinburgh (FRSE), IET, and China Institute of Communications, an IEEE Communications Society Distinguished Lecturer in 2019 and 2020, a Highly-Cited Researcher recognized by Clarivate Analytics in 2017 and 2020. He was the recipient of 15 Best Paper Awards from IEEE Global Communications Conference (GLOBECOM) 2010, IEEE International Conference on Communication Technology (ICCT) 2011, International Conference on Intelligent Transport System Telecommunications (ITST) 2012, IEEE Vehicular Technology Conference (VTC)-Spring 2013, International Wireless Communications and Mobile Computing Conference (IWCMC) 2015, IWCMC 2016, IEEE/CIC International Conference on Communications in China (ICCC) 2016, International Symposium on Wireless Personal Multimedia Communications (WPMC) 2016, Wireless and Optica Communications Conference (WOCC) 2019, IWCMC 2020, International Conference on Wireless Communications and Signal Processing (WCSP) 2020, International Conference on Communications, Signal Processing, and Systems (CSPS) 2021, WCSP 2021, and IEEE/CIC ICCC 2022. He was a TPC Member, the TPC Chair, and General Chair of more than 30 international conferences. He was also the Editor for more than ten international journals, including the IEEE TRANSACTIONS ON WIRELESS COMMUNICATIONS from 2007 to 2009, IEEE TRANSACTIONS ON VEHICULAR TECHNOLOGY from 2011 to 2017, and IEEE TRANSACTIONS ON COMMUNICATIONS from 2015 to 2017. He was the Guest Editor of the IEEE JOURNAL ON SELECTED AREAS IN COMMUNICATIONS, Lead Guest Editor of Special Issue on *Vehicular Communications and Networks*, Special Issue on *Spectrum and Energy Efficient Design of Wireless Communication Networks*, and Special Issue on *Airborne Communication Networks*. He was also the Guest Editor of the Special Issue on Wireless Big Data of the IEEE TRANSACTIONS ON BIG DATA. He is an Executive Editorial Committee Member of the IEEE TRANSACTIONS ON WIRELESS COMMUNICATIONS. He is also the Guest Editor of the Special Issue on Intelligent Resource Management for 5G and Beyond of the IEEE TRANSACTIONS ON COGNITIVE COMMUNICATIONS AND NETWORKING.

Jie Huang (Member, IEEE) received the B.E. degree in information engineering from Xidian University, Xi'an, China, in 2013, and the Ph.D. degree in information and communication engineering from Shandong University, Jinan, China, in 2018. From 2018 to 2020, he was a Postdoctoral Research Associate with National Mobile Communications Research Laboratory, Southeast University, Nanjing, China, supported by the National Postdoctoral Program for Innovative Talents. From 2019 to 2020, he was a Postdoctoral Research Associate with Durham University, Durham, U.K. Since 2019, he has been a part-time Researcher with Purple Mountain Laboratories, Nanjing. Since 2020, he has been an Associate Professor with National Mobile Communications Research Laboratory, Southeast University. He has authored and coauthored more than 80 papers in refereed journals and conference proceedings. His research interests include millimeter wave, massive MIMO, reconfigurable intelligent surface channel measurements and modeling, wireless Big Data, and 6G wireless communications. He was the recipient of the Best Paper Awards from WPMC 2016, WCSP 2020, and WCSP 2021. He has delivered 10 tutorials in IEEE/CIC ICCC 2021, IEEE PIMRC 2021, IEEE ICC 2022, IEEE VTC Spring 2022, IEEE/CIC ICCC 2022, IEEE VTC-Fall 2022, IEEE PIMRC 2022, IEEE Globecom 2022, IEEE WCNC 2023, and IEEE ICC 2023.

Ronghui Zhang (Member, IEEE) received the Ph.D. degree in information and communications engineering from the Beijing University of Posts and Telecommunications, Beijing, China, in 2021. He is currently a Research Fellow with the State Key Laboratory of Networking and Switching Technology, Beijing University of Posts and Telecommunications. His research interests include wireless sensing, integrated sensing and communications, edge intelligence, and application of machine learning and blockchain. He was a Member of the Technical Program Committee for a number of Flagship IEEE conferences, including IEEE GLOBECOM, IEEE ICC, IEEE/CIC ICCC, and IEEE WCNC. He was also the Lead Guest Editor of IET Signal Processing.